Journal of Applied Fluid Mechanics, Vol. 15, No. 3, pp. 737-745, 2022.
Available online at www.jafmonline.net, ISSN 1735-3572, EISSN 1735-3645.
https://doi.org/10.47176/jafm.15.03.33155

Multiscale Analysis of Hydrodynamic Step Bearing with Ultra Low Surface Separations

C. Cao and Y. Zhang†

College of Mechanical Engineering, Changzhou University, Changzhou, Jiangsu Province, China

†*Corresponding Author Email: engmech1@sina.com*

(Received July 5, 2021; accepted February 23, 2022)

ABSTRACT

The paper presents the multiscale analysis for the hydrodynamic step bearing with ultra low surface clearances where only the physical adsorbed layer is present in the outlet zone and the continuum fluid flow mainly occurs in the inlet zone. This bearing can occur under heavy loads. The flow in the outlet zone is described by the nanoscale flow equation, while the flow in the inlet zone is described by the multiscale flow equation incorporating both the adsorbed layer flow and the intermediate continuum fluid flow. The pressure and carried load of the bearing were derived. Exemplary calculations show that the fluid-bearing surface interaction has the strongest influence on the pressure and carried load of this bearing when the bearing surface clearance is as small as possible, the bearing step size is close to the surface clearance in the outlet zone and the value of the geometrical parameter ψ is the optimum one, which depends on the fluid-bearing surface interaction. For the strong fluid-bearing surface interaction, the carried load of the bearing can be 10 times higher than that calculated from the classical hydrodynamic lubrication theory.

Keywords: Bearing; Hydrodynamics; Load; Model; Multiscale; Pressure.

NOMENCLATURE

$a_0, a_1, a_2,$ $m_0, m_1, m_2, m_3,$ n_0, n_1, n_2, n_3	constant	P	dimensionless pressure, $ph_{tot,o}/u\eta_a$
Cy_1	$\eta_{bf,1}^{eff}/\eta$	p	pressure of the film
Cy_2	$\eta_{bf,2}^{eff}/\eta$	Q_m	dimensionless mass flow rate , $q_m/uh_{tot,o}\rho_a$
Cq_1	$\rho_{bf,1}^{eff}/\rho$	q_m	mass flow rate per unit contact length through the bearing
Cq_2	$\rho_{bf,2}^{eff}/\rho$	q_0	Δ_{j+1}/Δ_j (>1)
D	fluid molecule diameter	S	parameter accounting for the non-continuum effect across the surface separation in the outlet zone
$H_{bf,1}$	$h_{bf}/h_{cr,bf,1}$	u	sliding speed of the bearing
$H_{tot,o}$	$h_{tot,o}/h_{cr,bf,2}$	W	dimensionless load, $w/(u\eta_a)\,\lambda_{bf,i}$ h_{bf}/h_i
h_{bf}	thickness of the adsorbed layer	Δ_j	separation between the $(j+1)^{th}$ and j^{th} fluid molecules across the layer thickness
h_i	thickness of the continuum fluid film on the entrance of the bearing	Δh	step size of the bearing

$h_{tot,o}$	surface separation in the outlet zone	Δx	separation between the neighboring fluid molecules in the flow direction in the adsorbed layer
$h_{tot,i}$	surface separation in the inlet zone	Δ_{n-2}	separation between the neighboring fluid molecules across the layer thickness just on the adsorbed layer-fluid interface
$h_{cr,bf,1}$	critical thickness for characterizing the rheological properties of the adsorbed layer in the inlet zone	η	fluid bulk viscosity
$h_{cr,bf,2}$	critical thickness for characterizing the rheological properties of the boundary layer in the outlet zone	η_a	fluid bulk viscosity at ambient pressure
l_1 , l_2	widths of the outlet and inlet zones respectively	ρ	fluid bulk density
$\eta_{bf,1}^{eff}$	effective viscosity of the physical adsorbed layer in the inlet zone	ρ_a	fluid bulk density at ambient pressure
$\eta_{bf,2}^{eff}$	effective viscosity of the boundary layer across the whole surface separation in the outlet zone	$\rho_{bf,1}^{eff}$	average density of across the adsorbed layer thickness in the inlet zone
$\eta_{line,j-1}$	local viscosity between the j^{th} and $(j-1)^{th}$ fluid molecules across the layer thickness	$\rho_{bf,2}^{eff}$	average density across the whole surface separation in the outlet zone
n	equivalent number of the fluid molecules across the layer thickness	γ	exponent in the viscosity ratio formula

1. INTRODUCTION

Hydrodynamic slider bearings were designed according to the classical hydrodynamic lubrication theory (Pinkus and Sternlicht 1961), which is based on the continuum hydrodynamics. Continuum hydrodynamic models have been developed plentifully for these bearings in different operating conditions (Asada *et al*. 2007; Dwivedi *et al*. 2013; Machado and Cavalca 2015; Swanson 2005). They can be valid for relatively large bearing clearances where the effect of the adsorbed boundary layer on the bearing surface is negligible.

With the increases of the carried load, sliding speed or/and hydrodynamic film temperature, the hydrodynamic bearing will operate with very small bearing clearances where the thickness and effect of the adsorbed boundary layer should be considered. Particularly when the surface roughness is involved, in the local hydrodynamic area of the bearing, the surface separation can be comparable to the thickness of the adsorbed layer and the corresponding mixed lubrication analysis for the bearing should incorporate the adsorbed layer effect even for modest loads. It is disappointing that most of the previous research work did not consider these factors (Andharia *et al*. 2001; Maharshi *et al*. 2018; Naduvinamani *et al*. 2002; Prakash and Peeken 1985; Prasad *et al*. 2012; Siddangouda *et al*. 2014).

Another factor involving the adsorbed boundary layer effect should be the development of micro/nano slider bearings in micro electromechanical systems (MEMS), where the bearing clearance is essentially very small and the adsorbed boundary layer plays a vital role (Ho and Tai 1998; Judy 2001; Ramakrishnan *et al*. 2007). Classical hydrodynamic theories fail for micro/nano slider bearings, the analysis of which relies on the theory of physical adsorbed layer boundary lubrication (Zhang 2015a, b; Zhang and Pang 2015).

In the hydrodynamic slider bearing with normal geometrical configurations, when the load is critically heavy, the surface clearance will be very low so that physical adsorbed layer boundary lubrication occurs and classical hydrodynamic lubrication theory (Pinkus and Sternlicht 1961) fails. There have been a lot of theoretical modeling of hydrodynamic micro/nano slider bearings with very low surface clearances (Zhang 2015a, b; Zhang and Pang 2015; Qian *et al*. 2016, 2017). In those modeling, in the boundary lubrication area, the phase transition was treated as gradual across the surface separation (Zhang 2015a, b; Zhang and Pang 2015; Qian *et al*. 2016, 2017).

In recent years, Zhang proposed that when the surface separation is low enough, the lubrication in a hydrodynamic contact should first enter into the multiscale lubrication consisting of both the adsorbed layer flow and the intermediate continuum fluid flow (Zhang 2020). He presented the multiscale analysis for the hydrodynamic line contact in this condition (Zhang 2021). He also proposed that in the hydrodynamic line contact,

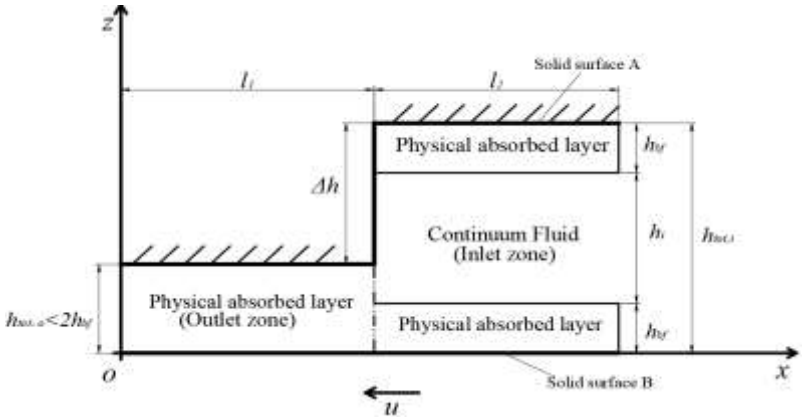

Fig. 1. Studied model of the hydrodynamic step bearing with the side leakage negligible.

when the surface separation is further reduced, the whole Hertzian contact zone will enter into the physical adsorbed layer boundary lubrication (with the continuum fluid film vanishing), while most of the inlet zone should be essentially in the multiscale lubrication with both the adsorbed layer and the intermediate continuum fluid participating in the flow (Zhang 2022). Lin *et al*. (2022) showed that for the hydrodynamic line contact with very low surface separations, for the same load, the surface separation calculated from the newly developed multiscale scheme (Zhang 2021, 2022) is very close to that calculated from the previously developed analytical method (Zhang 2015a, b; Zhang and Pang 2015; Qian *et al.* 2016, 2017) based on the continuous phase transition across the surface separation.

The present paper presents a new multiscale analysis for the hydrodynamic step bearing with very low surface separations by considering the outlet zone only in the physical adsorbed layer boundary lubrication and the inlet zone in the multiscale lubrication contributed by both the adsorbed layer and the intermediate continuum fluid. The studied bearing should occur under critically heavy loads. It is a more realistic model of the bearing. The present analysis is like the type shown by Zhang (2022). The obtained results for this particular bearing are fresh and of importance to properly understanding the behavior of the bearing.

The model presented in this study will also be indicative to the following researches of hydrodynamic slider bearings with very small surface clearances involving the surface roughness. It will help to develop the corresponding more advanced mixed lubrication model for these bearings by incorporating the adsorbed boundary layer effect. The results given in the present study can also be directly referenced when doing experiments on micro/nano step bearings or designing these bearings in the future.

2. MODEL OF THE BEARING

Figure 1 shows the model of the hydrodynamic step bearing studied in this paper, which is two-dimensional and has a negligible side leakage in the third dimension (i.e. in the y coordinate direction). In this bearing, the upper surface is stationary and the lower surface is moving with the speed u. When the bearing carries the load heavy enough, the bearing clearance in the outlet zone will be lower than the total thickness ($2h_{bf}$) of the two adsorbed layers on the bearing surfaces so that only physical adsorbed layer boundary lubrication occurs in this zone; while, because of the bearing step size Δh, in the inlet zone are still present the continuum fluid film with the thickness h_i, which is intermediate between the two adsorbed boundary layers. This is the model of multiscale mixed hydrodynamic step bearing, not addressed before.

The coupled bearing surfaces are assumed as identical, and the thicknesses of the adsorbed layers on the two bearing surfaces both are h_{bf}. For the present model of the bearing, the surface separation $h_{tot,o}$ in the outlet zone should be lower than $2h_{bf}$. The surface separation in the inlet zone is $h_{tot,i}$, and the widths of the outlet and inlet zones are respectively l_1 and l_2. The used coordinates are also shown in Fig. 1.

3. ANALYSIS

In the present study, the flow of the adsorbed boundary layer is described by the nanoscale flow equation, and the flow of the intermediate continuum fluid is described by the Newtonian fluid model. The interfacial slippage was assumed as absent on any interface. Also, the following conditions were assumed: (a) the film viscous heating effect is negligible and the case is isothermal; (b) the influences of the film pressure on the density and viscosity of the film both are negligible; (c) the bearing surfaces are perfectly smooth; (d) there are no flow in the y coordinate direction (not shown), i.e. there is a negligible side leakage in the bearing.

3.1 For the inlet zone

In this sub zone, the thickness h_{bf} of the adsorbed layer is comparable with the thickness h_i of the intermediate continuum fluid, and the effect of the adsorbed layer should be considered; there should

simultaneously occur the adsorbed layer flow and the intermediate continuum fluid flow, which are respectively in different flow regimes. There were ever the multiscale approaches to simulate the adsorbed layer and continuum fluid flows respectively by molecular dynamics simulation and the continuum fluid model (Atkas and Aluru 2002; Liu *et al.* 2007; Sun *et al.* 2010; Nie *et al.* 2004); however those schemes are not successfully applicable for the present case owing to the requirement of the over large computer storage and computational time. Zhang (2020, 2021, 2022) has developed the efficient multiscale scheme for the present multiscale flow problem by using the nanoscale flow equation to describe the adsorbed layer flow and assuming the rheology within the continuum fluid film to follow the Newtonian law. According to his method, the total mass flow rate per unit contact length through the bearing is (Zhang 2020, 2021, 2022):

$$q_m = -uh_{bf}\rho_{bf,1}^{eff} - \frac{uh_i}{2}\rho - \frac{h_i^3\rho}{12\eta}\frac{\partial p}{\partial x} + \frac{h_{bf}^3\rho_{bf,1}^{eff}}{\eta_{bf,1}^{eff}}\frac{\partial p}{\partial x}\left[\frac{F_1}{6} - \frac{\varepsilon}{1+\frac{\Delta x}{D}}\left(1+\frac{1}{2\lambda_{bf,i}} - \frac{q_0-q_0^n}{q_0^{n-1}-q_0^n}\frac{\Delta_{n-2}}{h_{bf}}\right)\right] + \frac{h_i^3\rho}{\eta_{bf,1}^{eff}}\frac{\partial p}{\partial x}\left[\frac{F_2\lambda_{bf,i}^2}{6} - \frac{\lambda_{bf,i}}{1+\frac{\Delta x}{D}}\left(\frac{1}{2}+\lambda_{bf,i} - \frac{q_0-q_0^n}{q_0^{n-1}-q_0^n}\frac{\Delta_{n-2}}{h_i}\right)\right] \quad (1)$$

where $\lambda_{bf,i} = h_{bf}/h_i$, u is positive, p is the film pressure, ρ and μ are respectively the bulk density and bulk viscosity of the fluid, $\rho_{bf,1}^{eff}$ and $\eta_{bf,1}^{eff}$ are respectively the average density and the effective viscosity of the physical adsorbed layer in the inlet zone, $\eta_{bf,1}^{eff} = Dh_{bf}/\left[(n-1)(D+\Delta_x)\left(\Delta_l/\eta_{line,l}\right)_{avr,n-1}\right]$, D and Δx are respectively the fluid molecule diameter and the separation between the neighboring fluid molecules in the x coordinate direction in the adsorbed layer, $q_0 = \Delta_{j+1}/\Delta_j$ (Δ_j is the separation between the $(j+1)^{th}$ and j^{th} fluid molecules across the layer thickness) and q_0 is constant, $\varepsilon = (2DI+II)/[h_{bf}(n-1)(\Delta_l/\eta_{line,l})_{avr,n-1}]$,

$F_1 = \eta_{bf,1}^{eff}(12D^2\Psi + 6D\Phi)/h_{bf}^3$,

$F_2 = 6\eta_{bf}^{eff}D(n-1)\left(l\Delta_{l-1}/\eta_{line,l-1}\right)_{avr,n-1}/h_{bf}^2$, 98 is the equivalent number of the fluid molecules across the layer thickness, and Δ_{n-2} is the separation between the neighboring fluid molecules across the layer thickness just on the adsorbed layer-fluid interface. Here,

$I = \sum_{i=1}^{n-1} i(\Delta_l/\eta_{line,l})_{avr,i}$, $\Psi = \sum_{i=1}^{n-1} j(l\Delta_{l-1}/\eta_{line,l-1})_{avr,j}$,

$II = \sum_{i=0}^{n-2}[i(\Delta_l/\eta_{line,l})_{avr,i} + (i+1)(\Delta_l/\eta_{line,l})_{avr,i+1}]\Delta_i$,

$\Phi = \sum_{i=0}^{n-2}[i(l\Delta_{l-1}/\eta_{line,l-1})_{avr,j} + (i+1)(l\Delta_{l-1}/\eta_{line,l-1})_{avr,j+1}]\Delta_i$,

$i(\Delta_l/\eta_{line,l})_{avr,i} = \sum_{j=1}^{i}\Delta_{j-1}/\eta_{line,j-1}$,

and $i(l\Delta_{l-1}/\eta_{line,l-1})_{avr,i} = \sum_{j=1}^{i} j\Delta_{j-1}/\eta_{line,j-1}$; $\eta_{line,j-1}$ is the local viscosity between the j^{th} and $(j-1)^{th}$ fluid molecules across the layer thickness, and $\eta_{line,j}/\eta_{line,j+1} = q_0^{\gamma}$. Integrating Eq. (1) gives that:

$$p(x) = \frac{\left(q_m + uh_{bf}\rho_{bf,1}^{eff} + \frac{uh_i}{2}\rho\right)x + c_1}{A_1} \quad (2)$$

where c_1 is an integral constant and

$$A_1 = -\frac{h_i^3\rho}{12\eta} + \frac{h_{bf}^3\rho_{bf,1}^{eff}}{\eta_{bf,1}^{eff}}\left[\frac{F_1}{6} - \frac{\varepsilon}{1+\frac{\Delta x}{D}}\left(1+\frac{1}{2\lambda_{bf,i}} - \frac{q_0-q_0^n}{q_0^{n-1}-q_0^n}\frac{\Delta_{n-2}}{h_{bf}}\right)\right] + \frac{h_i^3\rho}{\eta_{bf,1}^{eff}}\left[\frac{F_2\lambda_{bf,i}^2}{6} - \frac{\lambda_{bf,i}}{1+\frac{\Delta x}{D}}\left(\frac{1}{2}+\lambda_{bf,i} - \frac{q_0-q_0^n}{q_0^{n-1}-q_0^n}\frac{\Delta_{n-2}}{h_i}\right)\right] \quad (3)$$

Based on the boundary condition $p\big|_{x=l_1+l_2} = 0$, it is solved from Eq. (2) that:

$$c_1 = -(l_1+l_2)\left(q_m + uh_{bf}\rho_{bf,1}^{eff} + \frac{uh_i}{2}\rho\right) \quad (4)$$

The pressure in the inlet zone is thus:

$$p(x) = G_{1,i}(x)\cdot q_m + G_{2,i}(x) \quad for\ l_1 \le x \le l_1+l_2 \quad (5)$$

where $G_{1,i}(x) = \frac{x-(l_1+l_2)}{A_1}$ (6)

and $G_{2,i}(x) = \frac{x-(l_1+l_2)}{A_1}\left(uh_{bf}\rho_{bf,1}^{eff} + \frac{uh_i}{2}\rho\right)$ (7)

Equation (5) gives the pressure on the boundary between the inlet and outlet zones as:

$$p(l_1) = G_{1,i}(l_1)\cdot q_m + G_{2,i}(l_1) \quad (8)$$

3.2 For the outlet zone

In this sub zone, the surface separation is so low that the continuum fluid film disappears and only the adsorbed boundary layer remains. Here, the nanoscale flow equation (Zhang 2016) was used to describe the flow in this zone, rather than by using molecular dynamics simulation; the total mass flow rate per unit contact length through the bearing in this zone is:

$$q_m = -\frac{u}{2}h_{tot,o}\rho_{bf,2}^{eff} + \frac{S\rho_{bf,2}^{eff}h_{tot,o}^3}{12\eta_{bf,2}^{eff}}\frac{dp}{dx} \quad (9)$$

where $\rho_{bf,2}^{eff}$ and $\eta_{bf,2}^{eff}$ are respectively the average density and the effective viscosity of the adsorbed layer in the outlet zone, and S the parameter accounting for the non-continuum effect across the surface separation in the outlet zone.

Integrating Eq. (9) gives that:

$$p(x) = \frac{q_m x + \frac{u}{2} h_{tot,o} \rho_{bf,2}^{eff} x + c_2}{A_2} \tag{10}$$

where c_2 is an integral constant and

$$A_2 = \frac{S \rho_{bf,2}^{eff} h_{tot,o}^3}{12 \eta_{bf,2}^{eff}} \tag{11}$$

Based on the boundary condition $p|_{x=0} = 0$, it is solved from Eq.(10) that $c_2 = 0$. The pressure in the outlet zone is thus:

$$p(x) = G_{1,o}(x) q_m + G_{2,o}(x) \quad for\ 0 \le x \le l_1 \tag{12}$$

where

$$G_{1,o} = \frac{x}{A_2} \tag{13}$$

and

$$G_{2,o} = \frac{x u h_{tot,o} \rho_{bf,2}^{eff}}{2A_2} \tag{14}$$

Equation (12) gives the pressure on the boundary between the inlet and outlet zones as:

$$p(l_1) = G_{1.o}(l_1) \cdot q_m + G_{2,o}(l_1) \tag{15}$$

3.3 Mass flow rate and carried load of the bearing

Solving the coupled Eqs. (8) and (15) gives the mass flow rate per unit contact length through the bearing as:

$$q_m = \frac{G_{2,o}(l_1) - G_{2,i}(l_1)}{G_{1,i}(l_1) - G_{1,o}(l_1)} \tag{16}$$

The load per unit contact length carried by the bearing is:

$$\begin{aligned} w &= \int_0^{l_1+l_2} p dx \\ &= q_m \int_0^{l_1} G_{1,o}(x) dx + \int_0^{l_1} G_{2,o}(x) dx + q_m \int_{l_1}^{l_1+l_2} G_{1,i}(x) dx + \int_{l_1}^{l_1+l_2} G_{2,i}(x) dx \\ &= \frac{q_m l_1^2}{2A_2} + \frac{u h_{tot,o} \rho_{bf,2}^{eff} l_1^2}{4A_2} - \frac{q_m l_2^2}{2A_1} - \frac{l_2^2}{2A_1}(u h_{bf} \rho_{bf,1}^{eff} + \frac{u h_i}{2} \rho) \end{aligned} \tag{17}$$

3.4 Normalization

The following dimensionless parameters were defined:

$$\psi = \frac{l_1}{l_2}, \quad X = \frac{x}{l_1 + l_2}, \quad \alpha = \frac{h_{tot,o}}{l_1 + l_2}, \quad K = \frac{1}{\alpha},$$

$$r = \frac{h_i}{h_{tot,o}} = 1 + \frac{\Delta h - 2h_{bf}}{h_{tot,o}}, \quad P = \frac{p h_{tot,o}}{u \eta_a},$$

$$W = \frac{w}{u \eta_a}, \quad Q_m = \frac{q_m}{u h_{tot,o} \rho_a}, \quad H_{bf,1} = \frac{h_{bf}}{h_{cr,bf,1}},$$

$$H_{tot,o} = \frac{h_{tot,o}}{h_{cr,bf,2}}, \quad Cq_1 = \frac{\rho_{bf,1}^{eff}}{\rho_a}, \quad Cq_2 = \frac{\rho_{bf,2}^{eff}}{\rho_a},$$

$$Cy_1 = \frac{\eta_{bf,1}^{eff}}{\eta_a}, \quad Cy_2 = \frac{\eta_{bf,2}^{eff}}{\eta_a}, \quad \overline{G}_{1,i} = \frac{G_{1,i} \rho_a h_i^2}{\eta_a},$$

$$\overline{G}_{2,i} = \frac{G_{2,i} h_i}{u \eta_a}, \ \overline{G}_{1,o} = \frac{G_{1,o} \rho_a h_{tot,o}^2}{\eta_a}, \ \overline{G}_{2,o} = \frac{G_{2,o} h_{tot,o}}{u \eta_a}.$$

Here, ρ_a and η_a are respectively the bulk density and the bulk viscosity of the fluid at ambient condition, and $h_{cr,bf,1}$ and $h_{cr,bf,2}$ are respectively the critical film thicknesses for characterizing the rheological properties of the adsorbed boundary layers in the inlet and outlet zones.

3.4.1 For the present multiscale analysis

$\overline{G}_{1,i}$, $\overline{G}_{2,i}$, $\overline{G}_{1,o}$ and $\overline{G}_{2,o}$ are respectively expressed as:

$$\overline{G}_{1,i}(X) = \frac{K(X-1)}{rB_1} \tag{18}$$

$$\overline{G}_{2,i}(X) = \frac{K(X-1)}{rB_1}(\lambda_{bf,i} Cq_1 + \frac{1}{2}) \tag{19}$$

$$\overline{G}_{1,o}(X) = \frac{KX}{B_2} \tag{20}$$

$$\overline{G}_{2,o}(X) = \frac{KXCq_2}{2B_2} \tag{21}$$

where:

$$\begin{aligned} B_1 = &-\frac{1}{12} + \frac{Cq_1 \lambda_{bf,i}^3}{Cy_1} \left[\frac{F_1}{6} - \frac{\varepsilon}{1 + \frac{\Delta x}{D}} \left(1 + \frac{1}{2\lambda_{bf,i}} - \frac{q_o - q_o^n}{q_o^{n-1} - q_o^n} \frac{\Delta_{n-2}}{h_{bf}} \right) \right] \\ &+ \frac{1}{Cy_1} \left[\frac{F_2 \lambda_{bf,i}^2}{6} - \frac{\lambda_{bf,i}}{1 + \frac{\Delta x}{D}} \left(\frac{1}{2} + \lambda_{bf,i} - \frac{q_o - q_o^n}{q_o^{n-1} - q_o^n} \frac{\Delta_{n-2} \lambda_{bf,i}}{h_{bf}} \right) \right] \end{aligned} \tag{22}$$

$$B_2 = \frac{SCq_2}{12Cy_2} \tag{23}$$

The dimensionless mass flow rate per unit contact length through the bearing is:

$$Q_m = \frac{r^2 \overline{G}_{2,o} - r \overline{G}_{2,i}}{\overline{G}_{1,i} - r^2 \overline{G}_{1,o}} \tag{24}$$

The dimensionless pressure in the inlet zone is:

$$P(X) = \frac{Q_m}{r^2} \overline{G}_{1,i}(X) + \frac{\overline{G}_{2,i}(X)}{r} \quad for \frac{\psi}{\psi + 1} \le X \le 1 \tag{25}$$

The dimensionless pressure in the outlet zone is:

$$P(X) = Q_m \overline{G}_{1,o}(X) + \overline{G}_{2,o}(X) \quad for 0 \le X \le \frac{\psi}{\psi + 1} \tag{26}$$

The dimensionless load carried by the bearing is:

$$\begin{aligned} W = &\frac{K^2 Q_m}{2B_2} \left(\frac{\psi}{\psi + 1} \right)^2 + \frac{Cq_2 \psi^2 K^2}{4B_2 (\psi + 1)^2} \\ &- \frac{K^2 Q_m}{2r^3 B_1} \left(\frac{1}{\psi + 1} \right)^2 - \frac{K^2}{2r^2 B_1} \left(\lambda_{bf,i} Cq_1 + \frac{1}{2} \right) \left(\frac{1}{\psi + 1} \right)^2 \end{aligned} \tag{27}$$

3.4.2 For the conventional hydrodynamic lubrication theory

For comparison, the results calculated from the conventional hydrodynamic lubrication theory (Pinkus and Sternlicht 1961) are given as follows.

The dimensionless hydrodynamic film pressure in the bearing is:

$$P(X) = K(1 - X)(\frac{6}{r^2} + \frac{12 Q_{m,\ conv}}{r^3}) \quad for \frac{\psi}{\psi + 1} \le X \le 1 \tag{28}$$

$$P(X) = -KX(6 + 12 Q_{m,conv}) \quad for\ 0 \le X \le \frac{\psi}{\psi + 1} \tag{29}$$

where $Q_{m,conv} = -\frac{\psi r^2 + r}{2\psi r^3 + 2}$ (30)

The dimensionless carried load by the bearing is:

$$W = 3\left(\frac{K}{r(\psi+1)}\right)^2\left(1+\frac{2Q_{m,conv}}{r}\right) - 3\left(\frac{K\psi}{\psi+1}\right)^2\left(1+2Q_{m,conv}\right) \quad (31)$$

4. CALCULATION

The input parameter values for all the calculations are: $\Delta_{n-2}/D = 0.15$, $D = 0.5$ and $l_1 + l_2 = 20\mu m$. The parameters Cq_1 and Cq_2 are expressed as (Zhang 2021, 2022):

$$Cq_1(H_{bf,1}) = \begin{cases} 1 & , \quad for\ H_{bf,1} \geq 1 \\ m_0 + m_1 H_{bf,1} + m_2 H_{bf,1}^{\ 2} + m_3 H_{bf,1}^{\ 3}, & for\ 0 < H_{bf,1} \leq 1 \end{cases} \quad (32)$$

$$Cq_2(H_{tot,o}) \begin{cases} 1 & , \quad for\ H_{tot,o} \geq 1 \\ m_0 + m_1 H_{tot,o} + m_2 H_{tot,o}^{\ 2} + m_3 H_{tot,o}^{\ 3}, & for\ 0 < H_{tot,o} \leq 1 \end{cases} \quad (33)$$

where m_0, m_1, m_2 and m_3 are respectively constant.

The parameter Cy_1 and Cy_2 is expressed as (Zhang 2021, 2022):

$$Cy_1(H_{bf,1}) = \begin{cases} 1 & , \quad for\ H_{bf,1} \geq 1 \\ a_0 + a_1/H_{bf,1} + a_2/H_{bf,1}^{\ 2} & , \quad for\ 0 < H_{bf,1} \leq 1 \end{cases} \quad (34)$$

$$Cy_2(H_{tot,o}) = \begin{cases} 1 & , \quad for\ H_{tot,o} \geq 1 \\ a_0 + a_1/H_{tot,o} + a_2/H_{tot,o}^{\ 2} & , \quad for\ 0 < H_{tot,o} \leq 1 \end{cases} \quad (35)$$

where a_0, a_1 and a_2 are respectively constant.

The parameter S is expressed as (Zhang 2021, 2022):

$$S(H_{tot,o}) = \begin{cases} -1 & , \quad for\ H_{tot,o} \geq 1 \\ \left[n_0 + n_1\left(H_{tot,o} - n_3\right)^{n_2}\right]^{-1} & , \quad for\ n_3 \leq H_{tot,o} \leq 1 \end{cases} \quad (36)$$

where n_0, n_1 and n_2 are respectively constant.

F_1, F_2 and ε are respectively formulated as (Zhang 2020):

$$F_1 = 0.18\left(\Delta n - 2/D - 1.905\right)\left(\ln n - 7.897\right) \quad (37)$$

$$F_2 = -3.707\times10^{-4}\left(\Delta_{n-2}/D - 1.99\right)\left(n + 64\right)\left(q_0 + 0.19\right)\left(\gamma + 42.43\right) \quad (38)$$

$$\varepsilon = 4.56\times10^{-6}\left(\Delta_{n-2}/D + 31.419\right)\left(n + 133.8\right)\left(q_0 + 0.188\right)\left(\gamma + 41.62\right) \quad (39)$$

The weak, medium and strong fluid-bearing surface interactions were respectively considered. They respectively have the following characteristic parameter values:

For the weak interaction:

$h_{cr,bf,1}$ =7nm, $h_{cr,bf,2}$ =14nm, γ =0.5, n=3, q_0 =1.05, h_{bf} =1.65nm

For the medium interaction:

$h_{cr,bf,1}$ =20nm, $h_{cr,bf,2}$ =40nm, γ =1.0, n=5, q_0 =1.1, h_{bf} =2.76nm

For the strong interaction:

$h_{cr,bf,1}$ =40nm, $h_{cr,bf,2}$ =80nm, γ =1.5, n=8, q_0 =1.2, h_{bf} =4.32nm

The other characteristic parameter values for these interactions are respectively shown in Tables 1-3.

Table 1 Fluid viscosity data for different fluid-bearing surface interactions (Zhang 2021, 2022)

Parameter / Interaction	a_0	a_1	a_2
Strong	1.8335	-1.4252	0.5917
Medium	1.0822	-0.1758	0.0936
Weak	0.9507	0.0492	1.6447E-04

Table 2 Fluid density data for different fluid-bearing surface interactions (Zhang 2021, 2022)

Parameter / Interaction	m_0	m_1	m_2	m_3
Strong	1.43	-1.723	2.641	-1.347
Medium	1.30	-1.065	1.336	-0.571
Weak	1.116	-0.328	0.253	-0.041

Table 3 Fluid non-continuum property data for different fluid-bearing surface interactions (Zhang 2021, 2022)

Parameter / Interaction	n_0	n_1	n_2	n_3
Strong	0.4	-1.374	-0.534	0.035
Medium	-0.649	-0.343	-0.665	0.035
Weak	-0.1	-0.892	-0.084	0.1

5. RESULTS

5.1 Pressure distribution

Figure 2 compares the pressure distributions in the present multiscale mixed hydrodynamic bearing for different fluid-bearing surface interactions when Δh =8nm, ψ =1, and $h_{tot,o}$ =2.9nm; those pressure distributions are also compared with that calculated from classical hydrodynamic lubrication theory for the same case. It is strongly indicated that in the multiscale mixed hydrodynamic regime the pressure in the bearing is very significantly increased with the increase of the interaction strength between the fluid and the bearing surface; the weak fluid-bearing surface interaction gives the pressures in the bearing close to the classical hydrodynamic theory calculation; however for the strong fluid-bearing surface interaction, the maximum pressure in the bearing is more than 10 times that calculated from classical hydrodynamic lubrication theory.

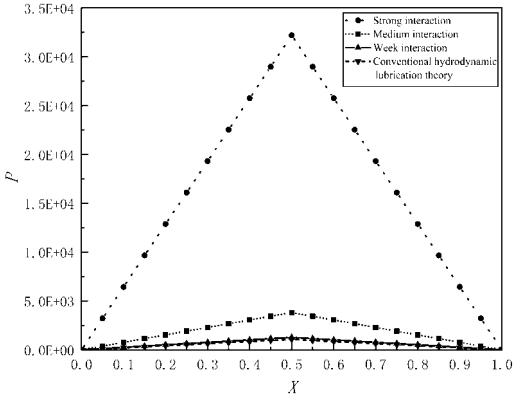

Fig. 2. Dimensionless pressure distributions in the present model of the bearing for different fluid-bearing surface interactions when Δh =8nm, ψ =1, and $h_{tot,o} = 2.9nm$.

5.2 Carried load of the bearing

Figure 3(a) plots the dimensionless carried loads of the bearing against the dimensional surface separation $h_{tot,o}$ in the outlet zone respectively for different fluid-bearing surface interactions when Δh =8nm and ψ =1; for the comparison purpose, for the present multiscale mixed hydrodynamic bearing, the value of $h_{tot,o}$ is limited to the very narrow range 2.8nm~3.3nm. For the same bearing clearance ($h_{tot,o}$), the carried load of the bearing is very significantly increased with the increase of the interaction strength between the fluid and the bearing surface; The weak fluid-bearing surface interaction has a negligible interaction effect on the carried load of the bearing, while the strong fluid-bearing surface interaction gives the carried load of the bearing more than 10 times that calculated from classical hydrodynamic lubrication theory.

Figures 3(b)-(d) respectively plot the dimensionless carried loads of the bearing against the dimensional surface separation $h_{tot,o}$ in the outlet zone for wider values when the fluid-bearing surface interaction is weak, medium or strong. In these figures, the multiscale mixed hydrodynamic regime refers to the present mode of the bearing, while the multiscale hydrodynamic regime refers to the mode of the bearing where the value of $h_{tot,o}$ is sufficiently large

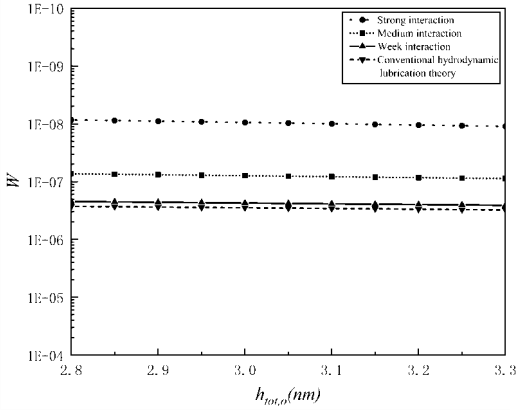

(a) Comparison for different interactions

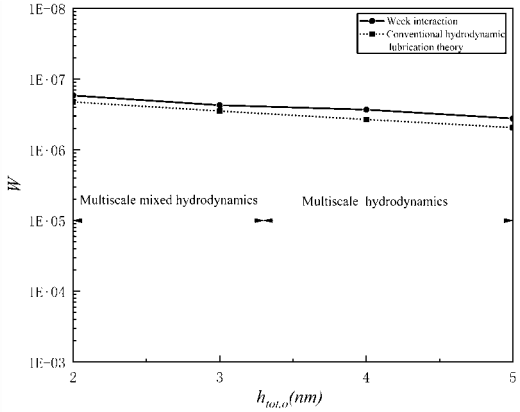

(b) Extended hydrodynamic regimes for the weak interaction

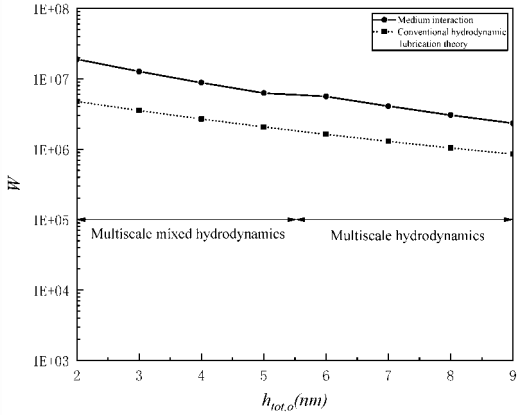

(c) Extended hydrodynamic regimes for the medium interaction

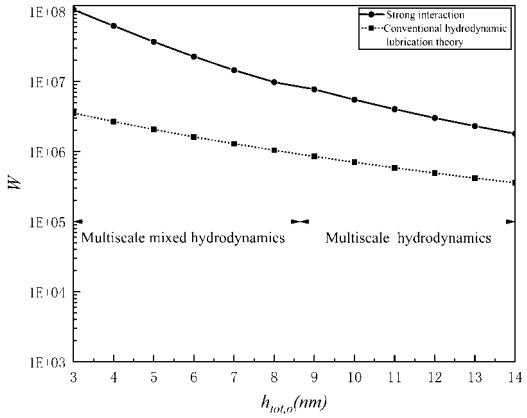

(d) Extended hydrodynamic regimes for the strong interaction

Fig. 3. Plots of the dimensionless carried load of the bearing against the outlet surface separation $h_{tot,o}$ for different fluid-bearing surface interactions when Δh =8nm and ψ =1.

so that there is the continuum fluid film intervening between the coupled adsorbed layers throughout the bearing, which has been studied by Shao and Zhang (2020). These figures show the much wider pictures where the load of the bearing is varied with $h_{tot,o}$. The strong fluid-bearing surface interaction is shown to have the strongest effect on the carried load of the bearing; this effect is more significant for a lower value of $h_{tot,o}$.

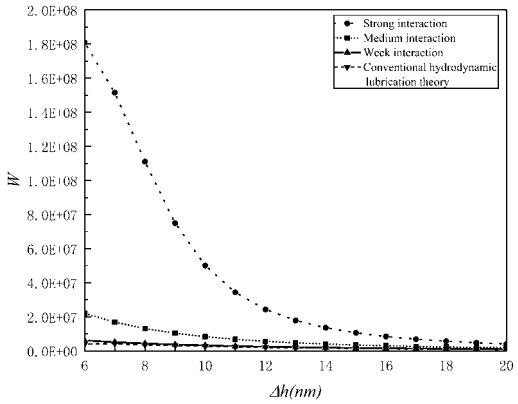

Fig.4 Variations of the dimensionless carried load of the bearing with the bearing step size Δh for different fluid-bearing surface interactions when ψ =1 and $h_{tot,o}$ =2.9nm.

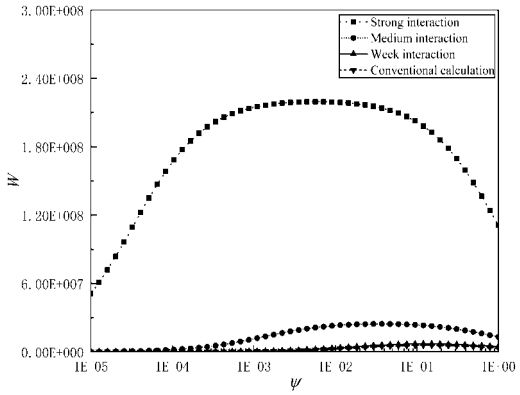

Fig. 5. Variations of the dimensionless carried load of the bearing with ψ respectively for different fluid-bearing surface interactions when Δh =8nm and $h_{tot,o}$ =2.9nm.

Figure 4 shows the variations of the carried load of the present mode of the bearing with the bearing step size Δh respectively for different fluid-bearing surface interactions when ψ =1 and $h_{tot,o}$ =2.9nm. The minimum value of Δh can only be around 6.0nm; further lower values of Δh will result in the failure of the present analysis. It is shown that over large Δh values make the interaction effect weak.

Figure 5 shows that there is the optimum value of ψ for which the effect of the fluid-bearing surface interaction is the strongest in the present model of the bearing. The curve for the weak fluid-bearing surface interaction is overlaid with that for the conventional hydrodynamic calculation. This optimum ψ value depends on the fluid-bearing surface interaction. For the weak fluid-bearing surface interaction, it is 0.13 and very close to that calculated from the classical hydrodynamic theory (Pinkus and Sternlicht 1961); for the medium interaction, it is 0.03; for the strong interaction, it is 0.005. The deviating of the value of ψ from this optimum one weakens the effect of the fluid-bearing surface interaction.

6. COMMENTING REMARKS

The addressed bearing has the ultra low surface separations which are only on the 1nm scale. Experimental results on this bearing are still scarce in the literature maybe owing to the high experimental technique requirement. Molecular dynamics simulation results for this bearing are also little seen because of the bearing too big size to simulate in the *x* coordinate direction. In spite of these, the results obtained in the present study will provide important indications for the following researches.

7. CONCLUSIONS

A new multiscale calculation was made for the mode of the hydrodynamic step bearing where only the adsorbed boundary layer is present in the outlet zone and there is the continuum fluid film intervening between the coupled adsorbed layers in the inlet zone. This mode of the bearing occurs for ultra low bearing clearances. Typical calculations manifest the following points:

(1) The fluid-bearing surface interaction has a very strong effect in this bearing; A strong fluid-bearing surface interaction greatly increases the load-carrying capacity of the bearing.

(2) There is the optimum value of the bearing geometrical parameter ψ for which the effect of the fluid-bearing surface interaction is the strongest. Also, smaller the bearing clearance, stronger the effect of the fluid-bearing surface interaction.

REFERENCES

Andharia, P. I., J. L. Gupta and G. M. Deheri (2001). Effect of Surface Roughness on Hydrodynamic Lubrication of Slider Bearings. *Tribology Transactions* 44, 291-297.

Asada, T., H. Saitou and D. Itou (2007). Design of hydrodynamic bearing for miniature hard disk drives. *IEEE Transactions on Magnetics* 43, 3721-3726.

Atkas, O. and N. R. Aluru (2002). A combined continuum/DSMC technique for multiscale analysis of microfluidic filters. *Journal of Computational Physics* 178,342-372.

Dwivedi, V. K., S. Chand and K. N. Pandey (2013). Effect of different flow regime on the static and dynamic performance parameter of hydrodynamic bearing. *Procedia Engineering* 51, 520-528.

Ho, C. M. and Y. C. Tai (1998). Micro-electro-mechanical-systems and fluid flows. *Annual Review of Fluid Mechanics* 30, 579-612.

Judy, J. W. (2001). Microelectromechanical systems (MEMS): fabrication, design and

applications. *Smart Materials and Structures* 10, 1115.

Lin, W., J. Li and Y. B. Zhang (2022). Comparison of the models for multiscale mixed hydrodynamics in a line contact. *Journal of Applied Fluid Mechanics*, 15, 515-521.

Liu, J., S. Chen, X. Nie and M. O. Robbins (2007). A continuum-atomistic simulation of heat transfer in micro- and nano- flows. *Journal of Computational Physics* 227, 279-291.

Machado, T. H. and K. L. Cavalca (2015). Modeling of hydrodynamic bearing wear in rotor-bearing systems. *Mechanics Research Communications* 69, 15-23.

Maharshi, K., T. Mukhopadhyay, B. Roy, L. Roy and S. Dey (2018). Stochastic dynamic behaviour of hydrodynamic journal bearings including the effect of surface roughness. *International Journal of Mechanical Sciences* 142-143, 370-383.

Naduvinamani, N. B., P. S. Hiremath and G. Gurubasavaraj (2002). Surface roughness effects in a short porous journal bearing with a couple stress fluid. *Fluid Dynamics Research* 31, 333.

Nie, X. B., S. Chen and M. O. Robbins (2004). A continuum and molecular dynamics hybrid method for micro- and nano- fluid flow. *Journal of Fluid Mechanics* 500, 55-64.

Pinkus, O. and B. Sternlicht (1961). *Theory of Hydrodynamic Lubrication.* McGraw-Hill, New York.

Prakash, J. and H. Peeken (1985). The combined effect of surface roughness and elastic deformation in the hydrodynamic slider bearing problem. *ASLE Transactions* 28, 69-74.

Prasad, E. S., T. Nagaraju and J. P. Sagar (2012). Thermohydrodynamic performance of a journal bearing with 3D-surface roughness and fluid inertia effects. *International Journal of Applied Research in Mechanical Engineering* 2, 18-24.

Qian, C., H. Wang, X. Jiang and Y. B. Zhang (2017). An abnormal nano step bearing constructed by physical adsorption. *Journal of the Balkan Tribological Association* 23, 158-165.

Qian, C., H. Wang, Y. Y. Zhu, X. Jiang and Y. B. Zhang (2016). A study on a Micro/nano step bearing with small steps. *Journal of the Balkan Tribological Association* 22, 2269-2283.

Ramakrishnan, N., E. C. Johns, Y. Zhao, J. D. Kiely and P. B. Chu (2007). Sliding contact micro-bearing for nano-precision sensing and positioning. *International Solid-State Sensors, Actuators and Microsystems Conference*, 9828809.

Shao, S. J. and Y. B. Zhang (2020). Study on multiscale hydrodynamic step bearing. *Journal of Modern Mechanical Engineering and Technology* 7, 66-73.

Siddangouda, A., T. V. Biradar and N. B. Naduvinamani (2014). Combined effects of micropolarity and surface roughness on the hydrodynamic lubrication of slider bearings. *Journal of the Brazilian Society of Mechanical Sciences and Engineering* 36, 45-58.

Sun, J., Y. He and W. Q. Tao (2010). Scale effect on flow and thermal boundaries in micro-/nano- channel flow using molecular dynamics-continuum hybrid simulation method. *International Journal For Numerical Methods In Engineering* 81, 207-228.

Swanson, E. (2005). Fixed-geometry, hydro-dynamic bearing with enhanced stability characteristics. *Tribology Transactions* 48, 82-92.

Zhang, Y. B. (2021). Multiscale hydrodynamics in line contacts. *Mechanics Research Communications* 111, 103658.

Zhang, Y. B. (2022). Multiscale mixed hydrodynamics in line contacts. *Continuum Mechanics and Thermodynamics* 34, 507-518.

Zhang, Y. B. (2020). Modeling of flow in a very small surface separation. *Applied Mathematical Modeling* 82, 573-586.

Zhang, Y. B. (2016). The flow equation for a nanoscale fluid flow. *International Journal of Heat and Mass Transfer* 92, 1004-1008.

Zhang, Y. B. and M. J. Pang (2015). An analysis of a concentric micro/nano journal bearing constructed by physical adsorption. *Journal of the Balkan Tribological Association* 21, 950-964.

Zhang, Y. B. (2015a). Novel nano bearings constructed by physical adsorption. *Scientific Reports* 5, 14539

Zhang, Y. B. (2015b). Parametric optimization of a nano slider bearing. *Journal of the Balkan Tribological Association* 21, 952-960.